Radiation and Absorption Losses of the Whispering-Gallery-Mode Dielectric Resonators Excited by a Dielectric Waveguide

Svetlana V. Boriskina, *Student Member, IEEE*, and Alexander I. Nosich, *Senior Member, IEEE*

***Abstract*— The scattering of a surface wave of a dielectric layer backed by a ground plane from the whispering-gallery-mode dielectric resonators is considered by use of the surface potential approach and analytical regularization. Efficient numerical algorithms have been developed with applications to the bandstop filter design. Transmitted and reflected power fractions and radiation and absorption losses are calculated and compared for two alternative field polarizations. The effect of excitation of the higher order modes of the waveguide is also studied.**

***Index Terms*— Analytical regularization, bandstop filters, dielectric resonators, losses.**

I. Introduction

SINCE THE 1960's, whispering-gallery-mode (WG) dielectric resonators (DR's) have been studied as important components of many optical and millimeter-wave electronic systems [1]–[8]. This is due to their advantages, e.g., not necessarily small size, high quality factor, mechanical stability, and capability of working in a wide frequency range from the microwave to visible radiation. The principle of operation of WG resonators is based on the excitation of a WG mode traveling along the resonator boundary and having the field oscillating between the boundary and an inner caustic. If the finite axial size of the resonator can be neglected and the excited field has no axial variation along the cylinder, the modes are separated to two independent families of E- and H-polarized ones, called WGH and WGE modes, respectively. WG DR's can be excited in various ways. In optical and millimeter-wave range, the most common practice is to use open surface-wave transmission lines, e.g., a dielectric waveguide or a microstrip line. When a resonator is coupled to a waveguide, the WG resonances cause the resonances in the transmission coefficients of the guided modes that offer an opportunity to design the bandstop filters.

At first, the simulation of the surface modes of the open waveguides scattered from cylindrical DR's was based on approximate theories. In [3] and [4], the WG resonators as bandstop filters in the image guide have been discussed, coupling coefficients between the guide and resonator have been approximately estimated, and some experimental results have been presented. In [7], the coupling was considered as a sequence of reflections of a cylinder-scattered field from the surface of the waveguide; only two interactions were taken into account. Meanwhile, today's trends, aimed at excluding costly time-and-material prototyping, call for the quick desktop "what if?" design tools, which are based on reliable analysis methods. A high and controlled accuracy is especially important if studying the millimeter-wave applications instead of optical ones because here the device dimensions are comparable to the wavelength [5], [6]. In view of this, the coupling between the resonator and waveguide must be taken into account in an adequate manner. An accurate way of studying the two-dimensional (2-D) problems of WGE- and WGH-mode resonators excited by a dielectric waveguide was offered in [8] by using the surface integral equation (IE) approach and the Green's function of a regular waveguide. An equivalent-volume IE approach was used in [9] to analyze a similar problem of cylindrical inhomogeneity inside a waveguide. In [10], a generalized set of surface-potential IE's was derived for the scattering from an arbitrarily shaped cylindrical inhomogeneity, and a solution algorithm was proposed based on the inversion of the static part of the IE.

However, all the mentioned theoretical works did not study specific microwave applications such as filtering. This has been addressed in [11] for a 2-D circular DR and slitted metal cavity filters in the single-mode open waveguide. As such a simplified waveguide, we took an impedance plane in the H-polarization case. The analysis method was based on the surface-potential IE's and analytical regularization. This guaranteed the convergence and controlled accuracy of computations even at sharp resonances, unlike the conventional moment method and finite-element techniques [12]. It was shown that WG filters have quite an observable radiation, which is maximum at the resonant frequencies, in sharp contrast to the common belief that WG resonators have negligible radiation losses [3], [4]. However, all the mentioned studies, including [11], dealt with the lossless dielectrics and, thus, did not estimate the absorption inside the resonators. Therefore, it is important to study the tradeoff between the radiation and absorption losses

Manuscript received March 20, 1998. This work was supported under a 1996 SUMMA Foundation Graduate Fellowship. The work of S. V. Boriskina was supported under a 1997 IEEE MTT-S Graduate Scholarship. The work of A. I Noshich was supported under a NATO-CNR Guest Fellowship.

S. V. Boriskina is with the Radio Physics Department, Kharkov State University, Kharkov 310077, Ukraine.

A. I. Nosich is with the Institute of Radio Physics and Electronics, Ukrainian Academy of Sciences, Kharkov 310085, Ukraine.

Publisher Item Identifier S 0018-9480(99)01146-1.

in a realistic model of a WG filter and compare both WGH- and WGE-mode cases.

This is the main goal of this paper. We used the same IE approach as in [11], which is equivalent and has some common features with [8] and [10]. It does not operate with "discrete plus continuous spectrum" expansions, but is based on the Fourier-integral expansions in terms of longitudinal wavenumber, understood in the sense of distributions due to the presence of guided-wave poles. We generalized the solution of [11] for modeling the WGE and WGH filters in a realistic multimode dielectric-slab waveguide backed by a ground plane. We also modified it for the tubular WG resonators that are frequently used to minimize the device weight.

This paper is organized as follows. In Section II, we briefly recall the main analysis results concerning the guided modes of a regular dielectric waveguide. In Section III, we derive the surface IE's for both of the polarization cases and convert them into the Fredholm second-kind infinite-matrix equations. This procedure, known as analytical regularization, is based on the inversion of the free-space part of the full IE operator, which involves a corresponding electric or magnetic 2-D Green's function of the regular dielectric waveguide. In Section IV, we present the formulas for the radiation field, mode-conversion coefficients, and absorption power, and power conservation law is discussed as well. Section V contains sample numerical results and a discussion of filter performance. Conclusions are summarized in Section VI. Time dependence is assumed as $e^{-i\omega t}$ and is omitted throughout this paper.

II. Natural Guided Modes of the Dielectric Slab Backed by a Ground Plane

All the guided surface-wave modes of a dielectric slab backed by a ground plane are known to split in two independent families of the E-polarized (TE_n) and H-polarized (TM_n) modes. Suppose that the thickness of the slab is d and the relative dielectric constant is ϵ_s (Fig. 1). The z-component of the field of any guided mode is then known to be one of the following:

$$E_z = E_n^{\pm}(x,y) \equiv V_n^E(y) e^{\pm ikh_n x}, \qquad n = 1,2,\cdots,Q^E \tag{1}$$

$$V_n^E(y) = \begin{cases} \sin(k\gamma_n d) e^{-k\rho_n(y+b)}, & -b < y < \infty \\ \sin[k\gamma_n(y+b+d)], & -(b+d) \le y \le -b \end{cases} \tag{2}$$

or

$$H_z = H_n^{\pm}(x,y) \equiv V_n^H(y) e^{\pm ikh_n x}, \qquad n = 0,1,\cdots,Q^H \tag{3}$$

$$V_n^H(y) = \begin{cases} \cos(k\gamma_n d) e^{-k\rho_n(y+b)}, & -b < y < \infty \\ \cos[k\gamma_n(y+b+d)], & -(b+d) \le y \le -b \end{cases} \tag{4}$$

where the upper index $E(H)$ corresponds to the (E)–(H) polarization, respectively, the upper index $\pm$ denotes the right/left moving waves $\rho_n = \sqrt{h_n^2 - 1}, \gamma_n = \sqrt{\epsilon_s - h_n^2}$. Guided modes having the propagation constants kh_n are counted from one in the E-case and from zero in the H-case, to emphasize that the lowest TM_0 guided mode has no cutoff and propagates at any frequency. Dimensionless numbers h_n form a finite set on the interval $1 < h_n < \sqrt{\epsilon_s}$ and are found as the real-value roots of one of the following dispersion equations:

$$D^E(h) \equiv \rho \sin(k\gamma d) + \gamma \cos(k\gamma d) = 0 \tag{5}$$

$$D^H(h) \equiv \epsilon_s \rho \cos(k\gamma d) - \gamma \sin(k\gamma d) = 0. \tag{6}$$

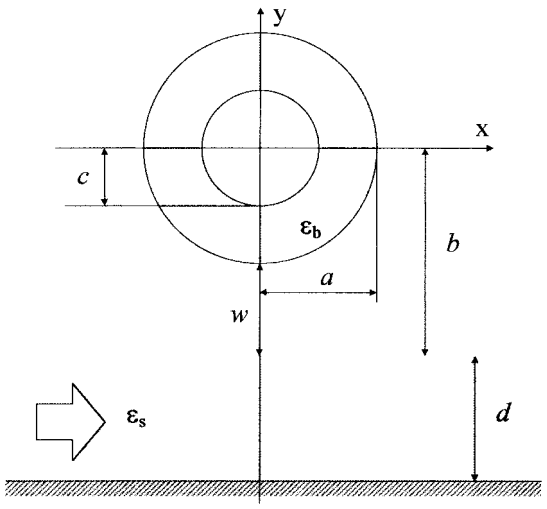

Fig. 1. Geometry of the scattering problem.

Functions (2) and (4) are normalized by using the relations as

$$\begin{aligned} (N_n^E)^2 &= kh_n \int_{-(b+d)}^{\infty} [V_n^E(y)]^2 \, dy \\ &= \frac{h_n kd}{2} + \frac{h_n}{2\rho_n} \end{aligned} \tag{7}$$

$$\begin{aligned} (N_n^H)^2 &= kh_n \int_{-(b+d)}^{\infty} \frac{1}{\epsilon(y)} [V_n^H(y)]^2 \, dy \\ &= \frac{h_n kd}{2\epsilon_s} + \frac{h_n}{2\rho_n [h_n^2(\epsilon_s + 1) - \epsilon_s]}. \end{aligned} \tag{8}$$

A norm is connected with the power carried by the nth surface-wave mode as $P^E = (1/2kZ_0)(N_n^E)^2$ or $P^H = (Z_0/2k)(N_n^H)^2$, respectively, with Z_0 for the free-space impedance.

III. Derivation and Solution of IE's

Consider now a tubular DR with a complex relative dielectric constant ϵ_b excited by a guided mode of the dielectric layer backed by a ground plane, as shown in Fig. 1. We shall assume that the fields do not vary along the z-axis, thus, the problem is a 2-D one. The outer and inner radii of the ring are denoted as a and c, respectively. The layer separation from the cylinder is w, so that the latter center is at the distance $b = w + a$ from the layer.

The total field in such a geometry can be characterized by the single scalar function U, which represents either E_z or H_z component, depending on the polarization. It can be written as

$$U = \begin{cases} U^{\mathrm{inc}} + U^{sc}, & r > a \\ U^{\mathrm{res}}, & a < r < c \\ U^{\mathrm{ins}}, & r < c \end{cases} \tag{9}$$

where $U^{\rm inc}$ is equal either to E_n^+ or H_n^+, given by (1) or (3), respectively.

The total field must satisfy the Helmholtz equation, with corresponding coefficients in each material, the boundary conditions on the contours L_a and L_c, and on the waveguide boundaries, and a modified radiation condition that is, according to [13],

$$U^{sc}(\vec{r}) \underset{r\to\infty}{\sim} \left\{ \begin{matrix} \Phi^{E(H)}(\varphi)(2/i\pi kr)^{1/2}e^{ikr}, y>-b \\ 0, y\le -b \end{matrix} \right\} + \sum_{n=1(0)}^{Q^{E(H)}} \left\{ \begin{matrix} T_n^{E(H)}-\delta_{sn}, x>0 \\ R_n^{E(H)}, x<0 \end{matrix} \right\} V_n^{E(H)}(y)e^{ih_n|x|}. \quad (10)$$

Here, δ_{sn} is the Kronecker delta, s is the index of the incident guided wave $1(0)\le s\le Q^{E(H)}$, where $Q^{E(H)}$ is the total number of the higher order guided modes supported by the slab at the given frequency. Function $\Phi^{E(H)}(\varphi)$ is the far-field radiation pattern of the discontinuity, and numbers $T_n^{E(H)}$ and $R_n^{E(H)}$ are the mode conversion coefficients. If $n=s$, they can be considered as the transmission and reflection coefficients of the incident guided mode.

Representing all the fields in terms of the single-layer surface potentials (*) see a critical comment below

$$U^{sc}(\vec{r}) = \int_{L_a} \psi^{E(H)}(\vec{r}_a)G_w^{E(H)}(\vec{r},\vec{r_a})\,dl_a \quad (11)$$

$$U^{\rm res}(\vec{r}) = \int_{L_a} \varphi^{E(H)}(\vec{r}_a)G_\epsilon^{E(H)}(\vec{r},\vec{r_a})\,dl_a + \int_{L_c} \mu^{E(H)}(\vec{r}_c)G_\epsilon^{E(H)}(\vec{r},\vec{r_c})\,dl_c \quad (12)$$

$$U^{\rm ins}(\vec{r}) = \int_{L_c} \beta^{E(H)}(\vec{r}_c)G_0(\vec{r},\vec{r_c})\,dl_c \quad (13)$$

and using the boundary conditions on the ring surfaces, we obtain the following set of four coupled IE's for the unknown density functions [upper index $E(H)$ is omitted]:

$$\int_{L_a} \varphi(\vec{r}_a)G_\epsilon(\vec{r},\vec{r}_a)\,dl_a + \int_{L_c} \mu(\vec{r}_c)G_\epsilon(\vec{r},\vec{r}_c)\,dl_c = \int_{L_a} \psi(\vec{r}_a)G_w(\vec{r},\vec{r}_a)\,dl_a + U^{\rm inc}(\vec{r}), \qquad \vec{r}\in L_a \quad (14)$$

$$\frac{1}{\alpha}\frac{\partial}{\partial n}\left\{\int_{L_a} \varphi(\vec{r}_a)G_\epsilon(\vec{r},\vec{r}_a)\,dl_a + \int_{L_c} \mu(\vec{r}_c)G_\epsilon(\vec{r},\vec{r}_c)\,dl_c\right\} = \frac{\partial}{\partial n}\int_{L_a} \psi(\vec{r}_a)G_w(\vec{r},\vec{r}_a)\,dl_a + \frac{\partial}{\partial n}U^{\rm inc}(\vec{r}), \qquad \vec{r}\in L_a \quad (15)$$

$$\int_{L_a} \varphi(\vec{r}_a)G_\epsilon(\vec{r},\vec{r}_a)\,dl_a + \int_{L_c} \mu(\vec{r}_c)G_\epsilon(\vec{r},\vec{r}_c)\,dl_c = \int_{L_c} \beta(\vec{r}_c)G_0(\vec{r},\vec{r}_c)\,dl_c, \qquad \vec{r}\in L_c \quad (16)$$

$$\frac{1}{\alpha}\frac{\partial}{\partial n}\left\{\int_{L_a} \varphi(\vec{r}_a)G_\epsilon(\vec{r},\vec{r}_a)\,dl_a + \int_{L_c} \mu(\vec{r}_c)G_\epsilon(\vec{r},\vec{r}_c)\,dl_c\right\} = \frac{\partial}{\partial n}\int_{L_c} \beta(\vec{r}_c)G_0(\vec{r},\vec{r}_c)\,dl_c, \qquad \vec{r}\in L_c. \quad (17)$$

Here, the coefficient α takes the value of one in the E-polarization case or ϵ_b in the H-polarization case, $G_\epsilon^{E(H)}$ is the (E)–(H)-type Green's function of the homogeneous medium with permittivity ϵ_b, G_0 is the free-space Green's function, and $G_w^{E(H)}$ is the Green's function of the half-space bounded by a dielectric slab above a ground plane, i.e.,

$$G_\epsilon^{E(H)}(\vec{r},\vec{r}_a) = \alpha\frac{i}{4}H_0^{(1)}(k\sqrt{\epsilon_b}|\vec{r}-\vec{r}_a|)$$
$$G_0(\vec{r},\vec{r}_c) = \frac{i}{4}H_0^{(1)}(k|\vec{r}-\vec{r}_c|) \quad (18)$$

$$G_w^{E(H)}(\vec{r},\vec{r}_a) = G_0(\vec{r},\vec{r}_a) + \frac{i}{4\pi}\int_{-\infty}^{\infty} \frac{S^{E(H)}(h)}{gD^{E(H)}(h)} \cdot e^{igk(y+y_a+2b)+ihk(x-x_a)}\,dh \quad (19)$$

where $g=\sqrt{1-h^2}$, $\gamma=\sqrt{\epsilon_s-h^2}$, $D^{E(H)}(h)$ are given by (5) and (6) (note that $g=i\rho$), and

$$S^E(h) = ig\sin(k\gamma d)+\gamma\cos(k\gamma d)$$
$$S^H(h) = ig\epsilon_s\cos(k\gamma d)-\gamma\sin(k\gamma d). \quad (20)$$

For the case of a solid circular cylinder, only the first pair of the above IE's, i.e., (14) and (15), should be used, with $\mu^{E(H)}(\vec{r}_c)\equiv 0$.

We further recall that the free-space scattering from a circularly layered cylinder can be solved in explicit form leading to infinite series. This is due to the fact that the functions $\{e^{in\varphi}\}_{n=-\infty}^{\infty}$ form the set of orthogonal eigenfunctions of *all* the integral operators in (14)–(17) if the kernel function G_w in (14) and (15) (i.e., the Green's function of the slab waveguide) is replaced by its first (i.e., the free-space) term G_0. Explicitly,

$$\int_0^{2\pi} e^{in\varphi_a}H_0^{(1)}(2ka\sin\tfrac{1}{2}|\varphi-\varphi_a|)\,d\varphi_a = 2\pi J_n(ka)H_n^{(1)}(ka)e^{in\varphi}, \qquad n=0,\pm1,\cdots. \quad (21)$$

Using this set as expansion functions in the Galerkin-type discretization scheme, we can perform a partial analytical inversion, i.e., a regularization of our IE's. Note that unlike [10], this procedure involves an inversion of the frequency-dependent part corresponding to free-space circular cylinder. Thus, we expand the unknown functions as follows (upper index $E(H)$ is omitted):

$$\{\psi,\varphi\}(\vec{r}_a) = \frac{2}{i\pi a}\sum_{n=-\infty}^{\infty}\{x_n,\varphi_n\}e^{in\varphi_a}$$
$$\{\beta,\mu\}(\vec{r}_c) = \frac{2}{i\pi c}\sum_{n=-\infty}^{\infty}\{\beta_n,\mu_n\}e^{in\varphi_c} \quad (22)$$

and expand the kernel functions and the right-hand-side functions in (14)–(17) similarly to [11]. By using some algebra and the orthogonality of exponents in the term-by-term integrations, we exclude some of the unknowns and arrive at the following infinite-matrix equation for $X^{E(H)}=\{x_n^{E(H)}\}_{n=-\infty}^{\infty}$:

$$X^{E(H)} + C^{E(H)}X^{E(H)} = F^{E(H)} \quad (23)$$

where

(*) see below

$$C_{mn}^{E(H)} = \frac{i^{m-n} J_n(ka)\Omega_{m+n}^{E(H)}}{J_m(ka)\left[1+iB_m^{E(H)}\right]}$$

$$F_m^{E(H)} = \frac{e^{-\rho_s kb} f_s^{E(H)} i^m (h_s+\rho_s)^m}{J_m(ka)\left[1+iB_m^{E(H)}\right]} \tag{24}$$

$$f_s^E = \sin(k\gamma_s d)$$

$$f_s^H = \cos(k\gamma_s d) \tag{25}$$

$$\Omega_n^E = -H_n^{(1)}(2kb) + \frac{2i}{\pi}\int_{-\infty}^{\infty} \frac{\sin(k\gamma d)}{D^E(h)} \cdot (h-ig)^n e^{2igkb}\, dh \tag{26}$$

$$\Omega_n^H = -H_n^{(1)}(2kb) + \frac{2i\epsilon_s}{\pi}\int_{-\infty}^{\infty} \frac{\cos(k\gamma d)}{D^H(h)} \cdot (h-ig)^n e^{2igkb}\, dh \tag{27}$$

$$B_n^{E(H)} = W^{E(H)}\{J_n(ka\sqrt{\epsilon_b}), Y_n(ka)\}/\Delta_n^{E(H)} + A_n^{E(H)} W^{E(H)}\{Y_n(ka\sqrt{\epsilon_b}), Y_n(ka)\}/\Delta_n^{E(H)}$$

$$\Delta_n^{E(H)} = W^{E(H)}\{J_n(ka\sqrt{\epsilon_b}), J_n(ka)\} + A_n^{E(H)} W^{E(H)}\{Y_n(ka\sqrt{\epsilon_b}), J_n(ka)\} \tag{28}$$

$$A_n^{E(H)} = \frac{W^{E(H)}\{J_n(kc\sqrt{\epsilon_b}), J_n(kc)\}}{W^{E(H)}\{Y_n(kc\sqrt{\epsilon_b}), J_n(kc)\}}$$

$$W^{E(H)}\{f,g\} = \sqrt{\epsilon_b} f' g/\alpha - fg'. \tag{29}$$

J_n, Y_n are for the Bessel and Neumann functions, respectively, and the prime is for the derivative with respect to the argument.

The proof of the Fredholm second-kind nature of (23) for any $b>a$ can be done similarly to [8]. Due to this fact, it can be solved numerically with a guaranteed convergence to the exact values of unknowns. Convergence is understood here as a possibility to have a computation error progressively minimized down to machine precision by taking the greater truncation number. In the case of a solid circular cylinder ($c=0$), one should note that $A_n^{E(H)}=0$ in all the above equations.

IV. Far-Field Characteristics and Power Conservation

Obtaining the mode conversion coefficients is reduced, after the contour deformation in the complex h-plane, to calculating the residues at the poles $h=\pm h_n$ (see [11], [13]). We eventually find that

$$\begin{Bmatrix} T_n^{E(H)} - \delta_{sn} \\ R_n^{E(H)} \end{Bmatrix} = \frac{2e^{-\rho_n kb} f_n^{E(H)}}{(N_n^{E(H)})^2} \sum_{m=\infty}^{\infty} x_m^{E(H)} \cdot (\mp i)^m J_m(ka)(h_n \pm \rho_n)^m. \tag{30}$$

The far-field scattering pattern is evaluated by applying the steepest descent method in the far zone of the scatterer. This brings us to the following expressions:

$$\Phi^{E(H)}(\varphi) = \sum_{m=-\infty}^{\infty} x_m^{E(H)} (-i)^m J_m(ka) \cdot [e^{im\varphi} + R^{E(H)}(\varphi)\cdot e^{2ikb\sin\varphi - im\varphi}] \tag{31}$$

$$R^E(\varphi) = \frac{i\sin\varphi\sin(k\gamma d) + \gamma\cos(k\gamma d)}{i\sin\varphi\sin(k\gamma d) - \gamma\cos(k\gamma d)}$$

$$R^H(\varphi) = \frac{i\epsilon_s\sin\varphi\cos(k\gamma d) - \gamma\sin(k\gamma d)}{i\epsilon_s\sin\varphi\cos(k\gamma d) + \gamma\sin(k\gamma d)} \tag{32}$$

where $\gamma(\varphi) = \sqrt{\epsilon_s - \cos^2\varphi}$.

Far-field characteristics are coupled together by the power conservation law (sometimes also called the optical theorem) [13], [14]. In our problem, it has the following form:

$$1 = P_{\rm tr} + P_{\rm ref} + P_{\rm rad} + P_{\rm abs} \tag{33}$$

where the quantities in the right-hand-side part are the power fractions associated with transmission, reflection, free-space radiation loss, and absorption loss in the imperfect DR, respectively; all of them are normalized to the power carried by the incident guided mode. Omitting the upper index $E(H)$, they are found as

$$P_{\rm tr} = \frac{1}{N_s^2}\sum_{n=1(0)}^{Q^{E(H)}} N_n^2|T_n|^2 \quad P_{\rm ref} = \frac{1}{N_s^2}\sum_{n=1(0)}^{Q^{E(H)}} N_n^2|R_n|^2 \tag{34}$$

where N_s is the norm of the incident mode

$$P_{\rm rad} = \frac{2}{\pi N_s^2}\int_0^{\pi} |\Phi(\varphi)|^2\, d\varphi \tag{35}$$

and

$$P_{\rm abs} = \frac{2\pi ka}{N_s^2}\sum_{n=-\infty}^{\infty} J_n^2(ka)|\xi_n^{E(H)}|^2 \cdot {\rm Im}\left\{\frac{\sqrt{\epsilon_b}}{\alpha}\frac{J_n'(ka\sqrt{\epsilon_b}) + A_n^{E(H)}Y_n'(ka\sqrt{\epsilon_b})}{J_n(ka\sqrt{\epsilon_b}) + A_n^{E(H)}Y_n(ka\sqrt{\epsilon_b})}\right\} \tag{36}$$

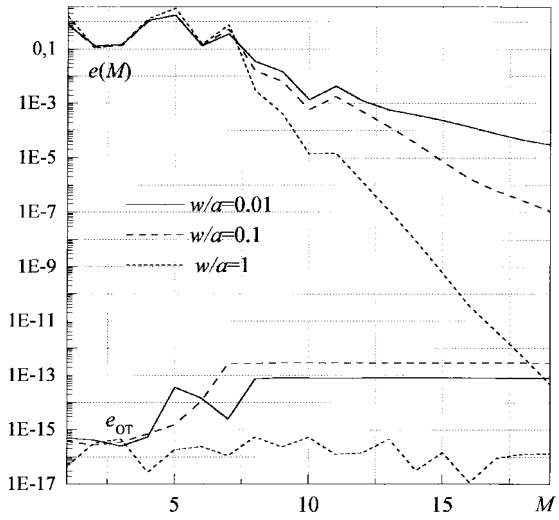

Fig. 2. Computation errors versus the matrix order for the WG DR $ka=5$, $\epsilon_b = 10 + 0.01i$, $d/a=1$, $\epsilon_s = 2.25$. ($e(M)$: matrix truncation error, $e_{\rm ot}$: optical theorem error).

(*) see below

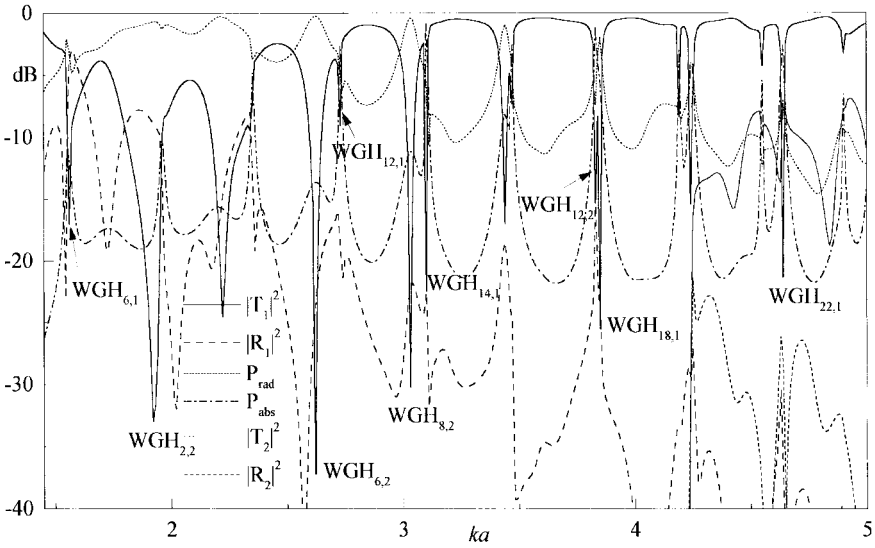

Fig. 3. Far-field scattering characteristics versus ka for the circular cylindrical DR (E-polarization case). $\epsilon_b = 10+0.01i$, $w/a = 0.01$, $d/a = 1$, $\epsilon_s = 2.25$.

where

$$\xi_n^{E(H)} = x_n^{E(H)} H_n^{(1)}(ka) + i^n \sum_{p=-\infty}^{\infty} x_p^{E(H)} (-i)^p J_p(ka) \cdot \Omega_{n+p}^{E(H)} + e^{-\rho_s kb} f_s^{E(H)} i^n (h_s + \rho_s)^n. \quad (37)$$

P_{abs} is calculated as a time-average power flow through the outer boundary of the cylinder (this flow is zero in the lossless case of $\operatorname{Im} \epsilon_b = 0$). Checking the balance of both sides of (33) may serve as a partial validation of the numerical code. After this, the power conservation law can be used to minimize the time needed to compute either P_{rad} or P_{abs}.

V. Numerical Results and Discussion

The Fredholm nature of the matrix equation (23) guarantees the convergence, but tells nothing about its rate. To make a reasonable estimation, we have plotted the error associated with the matrix truncation as a function of the truncation number M for the computation of the outer field (Fig. 2). This error is defined as follows:

$$e(M) = \frac{\max_{|n|\le M} |x_n^{M+1} - x_n^M|}{\max_{|n|\le M} |x_n^M|}. \quad (38)$$

It can be concluded that to have a fairly good three-digit accuracy, it is enough to take $M = ka + 3\sqrt[4]{a/w}$ for the each of two polarizations. As for the power conservation, it has been always satisfied with 10^{-12} or better accuracy (see Fig. 2); this is one of the merits of analytical regularization technique.

To fill the matrix, one has to compute the cylindrical functions and the functions $\Omega_n^{H(E)}$. The former, including those of a complex argument, were computed by a recursive code described in [15]. The latter need a numerical integration, which is one of the most time-consuming parts of the whole algorithm. On the initial contour of integration, i.e., on the real h-axis, there are two branch points $h = \pm 1$ and a finite number $2Q^E$ or $2(Q^H + 1)$, depending on the polarization of the poles at $h = \pm h_n$. To smooth the integrand and speed up computations, we follow the procedure proposed in [10]. First, we convert the integrals to the ones along the positive real semi-axis. The path of integration is then deformed to be composed of the four straight-line sections between the following points:

1) $h = 0$;
2) $h = -iT_a$;
3) $h = T_b - iT_a$;
4) $h = T_b$;
5) $h = T_c$;

where $T_a = 1/kb$, $T_b = \sqrt{\epsilon_s} + 1$. The location of the termination point depends on the rate of the integrand decay on the last segment and can be taken as $T_c = 15/kb$. Thus, the contribution of the poles is accounted for independently of their number, and the branch point is bypassed.

Central processing unit (CPU) time varied depending on the size of the scatterer. For example, computing a dielectric filter of $ka = 5$, $\epsilon_b = 10+0.01i$, and $w/a = 0.01$ with a three-digit accuracy needed $M = 12$; with a Pentium-100 MHz PC and double-precision MS-DOS Fortran source code it took 3 s.

Figs. 3 and 4 present the frequency dependences of the power fractions for the scattering from a circular solid cylindrical DR for the E- and H-polarizations, respectively. One can see that DR's can be used as bandstop filters in the surface-mode waveguides. The principle of operation of such filters is based on the excitation of the WG modes in the resonator. WG modes in the DR can be classified, according to [3] and [4] as $\text{WGE}_{m,n}$ or $\text{WGH}_{m,n}$ depending on the polarization. $\text{WGE(H)}_{m,n}$ modes correspond to the (H)–(E)-polarization case with the electric (magnetic) field being essentially tangential to the DR contour of cross section. The first subscript m denotes the number of the azimuthal field variations, the second n denotes the number of the radial variations. For various values of the waveguide parameters, a dielectric slab surface wave can excite various families of WG modes in the DR. For the waveguide thickness and

(*) see below

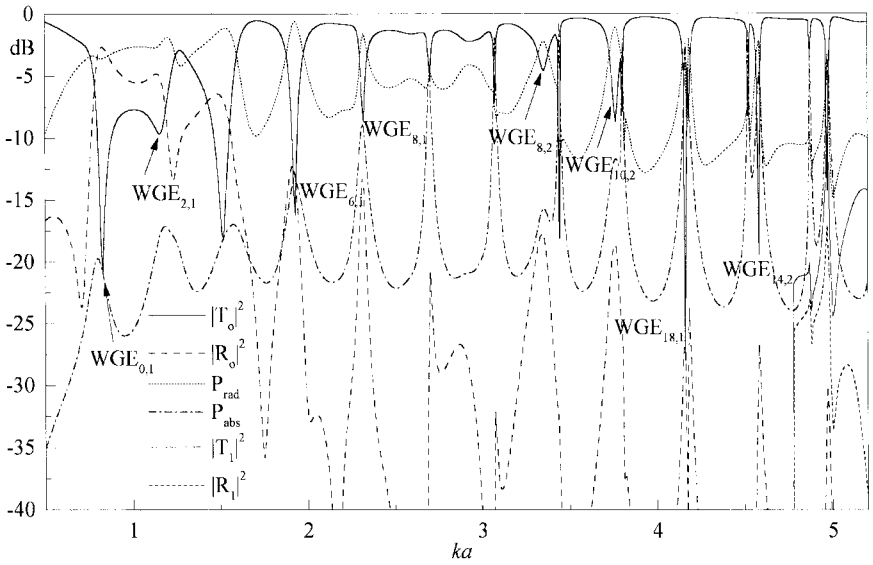

Fig. 4. Far-field scattering characteristics versus ka for the circular cylindrical DR (H-polarization case). $\epsilon_b = 10 + 0.01i$, $w/a = 0.01$, $d/a = 0.6$, $\epsilon_s = 2.25$.

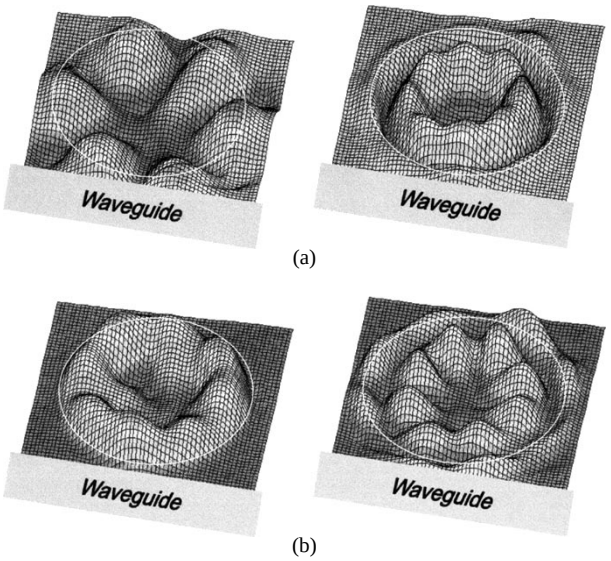

Fig. 5. The field spatial portraits inside DR's. (a) E-polarization: $\epsilon_b = 10 + 0.01i$, $w/a = 0.01$, $d/a = 1$, $\epsilon_s = 2.25$, $ka = 1.5585$ (left), and $ka = 3.0325$ (right). (b) H-polarization: $\epsilon_b = 10 + 0.01i$, $w/a = 0.01$, $d/a = 0.6$, $\epsilon_s = 2.25$, $ka = 2.317$ (left), and $ka = 3.349$ (right).

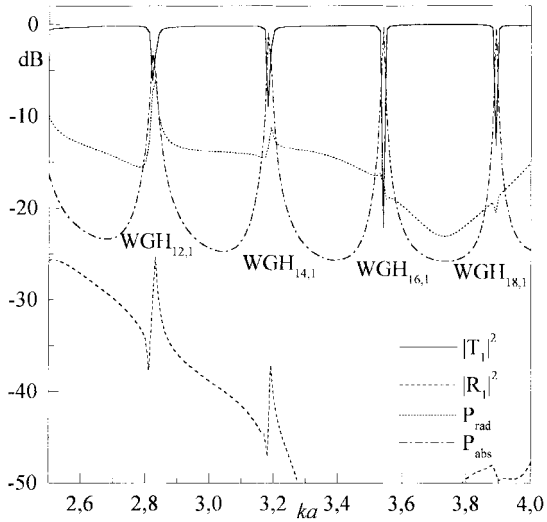

Fig. 6. Far-field scattering characteristics versus ka for the ring cylindrical DR (E-polarization case). $\epsilon_b = 10 + 0.01i$, $w/a = 0.01$, $d/a = 1$, $c/a = 0.7$, $\epsilon_s = 2.25$.

permittivity used in our numerical calculations, we observed excitation of two WG-mode families in the DR (with $n = 1$ and 2). The field spatial patterns inside the DR are depicted in Fig. 5, for the E-polarization (a), and for the H-polarization (b) cases, respectively. It must be noted that sometimes certain resonances are observed which can hardly be classified; the corresponding field is apparently formed by a mixture of two close natural oscillations.

Figs. 3 and 4 show that, in contrast to the common opinion that the radiation losses in the DR WG filter are negligible, most of the incident surface-mode power is either converted to the radiation field or absorbed inside the resonator. One can see that WGE modes show lower values of Q than corresponding WGH ones. This is in good agreement with experimental measurements of [6] and can be explained by the fact that to excite the WGE modes in the DR, a better coupling between the waveguide and resonator should be arranged. The coupling can be varied by choosing the distance between the DR and the waveguide [11, Fig. 4]. It is evident that we shift the resonance frequency when varying the distance w. It may be interesting to show how the resonant spectra of the DR loaded with a waveguide are shifted from the unloaded position. This analysis leads to an eigenvalue problem of seeking the complex-valued natural frequencies. Although it is formally based on the study of the homogeneous counterpart of (23), it is a more numerically complicated problem, thus, we do not consider it here.

To decrease the weight of the DR and to rarefy the WG-mode spectrum, which is rather dense, tubular dielectric cylinders can be used. Only the modes with a single radial variation are excited in a thin tubular DR (see Figs. 6 and 7). Parasitic-mode family $\mathrm{WGE(H)}_{m,2}$ is completely eliminated.

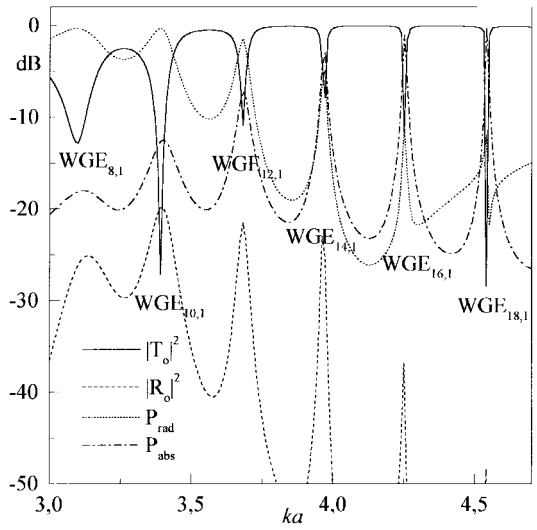

Fig. 7. Far-field scattering characteristics versus ka for the ring cylindrical DR (H-polarization case). $\epsilon_b = 10 + 0.01i$, $w/a = 0.01$, $d/a = 0.6$, $c/a = 0.7$, $\epsilon_s = 2.25$.

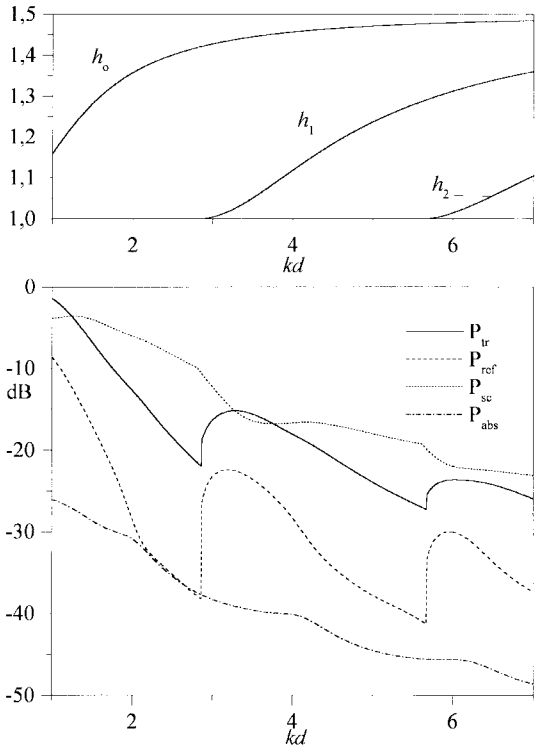

Fig. 8. Power fractions versus the waveguide thickness (E-polarization). $\epsilon_b = 10 + 0.01i$, $w/a = 0.01$, $c/a = 0.7$, $\epsilon_s = 2.25$, $ka = 3.25$.

Although, in most practical cases, a single-mode operation of the waveguide is desirable, it is interesting to study the effect of the newly born mode on the filter characteristics (Figs. 8 and 9). One can see that the appearance of a new surface mode causes an abrupt increase of the transmitted and reflected power fractions and a small decrease of the radiated and absorbed power fractions. Although these curves are continuous, their derivatives have square-root singularities at the cutoff frequencies of the higher order surface modes. This phenomenon has a threshold nature similar to the so-called

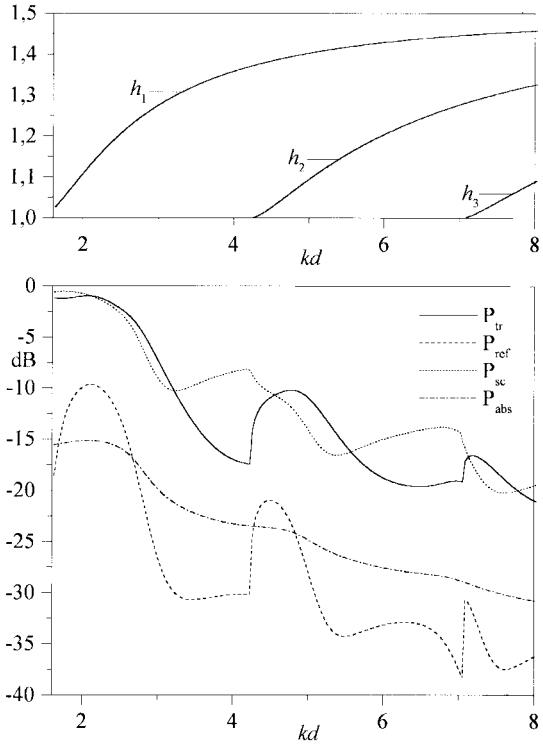

Fig. 9. Power fractions versus the waveguide thickness (H-polarization). $\epsilon_b = 10 + 0.01i$, $w/a = 0.01$, $c/a = 0.7$, $\epsilon_s = 2.25$, $ka = 1.0$.

Wood anomalies in the scattering of waves from periodic surfaces and closed-waveguide discontinuities.

VI. Conclusions

We have presented a numerically exact analysis method and modeling results concerning the surface-wave bandstop filters based on the 2-D WG cylindrical DR's. Reflection, transmission, radiated-field, and absorption characteristics were calculated for both E- and H-polarization cases.

Sharp resonant phenomena are observed for the scattering of guided modes from a dielectric cylinder in the form of periodic minima of the transmission coefficient at the WGE- and WGH-mode frequencies. Removing the dielectric material from the central part of the resonator does not effect the $\mathrm{WGE(H)}_{m,1}$ resonances unless the inner radius of the tubular resonator approaches the caustic, but eliminates parasitic $\mathrm{WGE(H)}_{m,2}$ resonances. Further thinning the ring undermines the Q-factor of the WG resonances due to a greater radiation. Both radiation and absorption powers reach maxima at the WG resonances, with the peak values depending on the loss tangent. What is remarkable is that the total dissipation losses $P_{\mathrm{rad}} + P_{\mathrm{abs}}$ are always greater than the power reflected by the WG filter. Thus, in reality, the analyzed device is a *dissipation filter* rather than a *rejection filter*, however small the loss tangent of the material used is. It has also been revealed that at the birth of a new surface mode, all the power characteristics experience an abrupt change and both P_{rad} and P_{abs} get smaller.

Note that due to the analytical regularization, our solutions are equally accurate off and near the sharp resonances, unlike the conventional numerical approximations [12]. This fact makes our algorithms well suited for the computer-aided

design of resonant microwave devices and points to a potential high efficiency of optimization software. It is worth noting that the presented approach can be easily extended to a multiresonator WG filter design. In combination with the dielectric-waveguide branching analyses, it can be applied to a design of a full WG diplexer.

ACKNOWLEDGMENT

The authors are thankful to K. Tanaka and A. G. Yarovoy for the helpful discussions. A. I. Nosich acknowledges the hospitality of Politecnico di Torino, Italy.

REFERENCES

[1] J. R. Wait, "Electromagnetic whispering gallery modes in a dielectric rod," *Radio Sci.*, vol. 2, no. 9, pp. 1005–1017, 1967.
[2] C. Vedrenne and J. Arnaud, "Whispering gallery modes of dielectric resonators," *Proc. Inst. Elect. Eng.*, vol. 129, pt. H, no. 4, pp. 183–187, 1982.
[3] X. H. Jiao, P. Guillon, L. A. Bermudez, and P. Auxemery, "Whispering-gallery modes of dielectric structures: Applications to millimeter-wave bandstop filters," *IEEE Trans. Microwave Theory Tech.*, vol. MTT-35, pp. 1169–1175, Dec. 1987.
[4] D. Cross and P. Guillon, "Whispering gallery dielectric resonator modes for W-band devices," *IEEE Trans. Microwave Theory Tech.*, vol. 38, pp. 1667–1673, Nov. 1990.
[5] Y. Filipov, S. Kharkovsky, and A. Kirichenko, "WG modes of nonuniform dielectric resonators," *Microwave Opt. Technol. Lett.*, vol. 10, no. 2, pp. 124–129, 1995.
[6] G. Annino, M. Cassetari, I. Longo, and M. Martinelli, "Whispering gallery modes in dielectric resonators: Characterization at the millimeter wavelengths," *IEEE Trans. Microwave Theory Tech.*, vol. 45, pp. 2025–2034, Nov. 1997.
[7] N. Morita, "Scattering and mode conversion of guided modes of a slab waveguide by a circular cylinder," *Proc. Inst. Elect. Eng.*, vol. 27, pt. H, no. 5, pp. 263–269, 1980.
[8] V. I. Kalinichev and P. N. Vadov, "A numerical investigation of the excitation of a dielectric resonator," *Soviet J. Commun. Technol. Electron.*, vol. 33, no. 7, pp. 108–115, 1988 (English transl.).
[9] N. K. Uzunoglu and J. G. Fikioris, "Scattering from an inhomogeneity inside a dielectric-slab waveguide," *J. Opt. Soc. Amer.*, vol. 72, no. 5, pp. 628–637, 1982.
[10] A. G. Yarovoy, "Surface potential method in the wave scattering from localized inhomogeneities of a planar dielectric waveguide," *IEICE Trans. Electron.*, vol. E 78-C, no. 10, pp. 1440–1446, 1995.
[11] S. V. Boriskina and A. I. Nosich, "Numerical simulation of surface-wave bandstop filters," *Microwave Opt. Technol. Lett.*, vol. 13, no. 3, pp. 169–173, 1996.
[12] G. L. Hower, R. G. Olsen, J. D. Earls, and J. B. Schneider, "Inaccuracies in numerical calculations of scattering near natural frequencies of penetrable objects," *IEEE Trans. Antennas Propagat.*, vol. 41, pp. 982–986, July 1993.
[13] A. I. Nosich, "Radiation conditions, limiting absorption principle, and general relations in open waveguide scattering," *J. Electromag. Waves Applicat.*, vol. 8, no. 3, pp. 329–353, 1994.
[14] P. G. Petropoulos and G. A. Kriegsmann, "Optical theorems for electromagnetic scattering by inhomogeneities in layered dielectric media," *IEEE Trans. Antennas Propagat.*, vol. 39, pp. 1119–1124, Aug. 1991.
[15] C. F. du Toit, "Evaluation of some algorithms and programs for the computation of integer-order Bessel functions of the first and second kind with complex arguments," *IEEE Antennas Propagat. Mag.*, vol. 35, pp. 19–25, Mar. 1993.

Svetlana V. Boriskina (S'96) was born in Kharkov, Ukraine, in 1973. She graduated from Kharkov State University, Kharkov, Ukraine, in 1995, and is currently working toward the Ph.D. degree at the same university.

Her research interests are in IE methods and electromagnetic-wave scattering from dielectric and metallic scatterers in layered media, with applications to open waveguides and antennas.

Alexander I. Nosich (M'94–SM'95) was born in Kharkov, Ukraine, in 1953. He graduated from Kharkov State University, Kharkov, Ukraine, in 1975, and received the Ph.D. and D.Sc. degrees in radio physics from the same university in 1979 and 1990, respectively.

Since 1978, he has been a Member of the Research Staff at the Institute of Radiophysics and Electronics (IRE), Ukrainian Academy of Sciences, Kharkov, Ukraine. From 1992 to 1998, he held research fellowships and Visiting Professorships in Bilkent University, Ankara, Turkey, Kumamoto University, Japan, Gifu University, Japan, and Chuo University, Tokyo, Japan, University of Rennes 1, France, and Torino Polytechnical University, Italy. He is currently with the Department of Computational Electromagnetics, IRE, as a Scientist. His research interests include free-space and open-waveguide scattering, complex-mode behavior, radar cross-section analysis, and antenna simulation.

(*) The field representation in terms of only the single-layer potential (11) is not the most general one. The same is true for the representation in terms of only the double-layer potential. Either of these representations leads to the appearance of the spurious (real-valued) eigenvalues of resulting IE that spoil the algorithm because the IE condition number has poles at the spurious-eigenvalue frequencies. The lowest of them, as can be easily found, lies near to the value where the largest "diameter" of the scatterer equals to one-half of the free-space wavelength. The severity of assocoated numerical error depends, however, on the details of the IE discretization scheme used.

If it is a MAR-based scheme as in the current paper, then the error is inacceptably large only in the domain of the width of the same order as MAR's error and can be compressed to machine-precision size by taking the matrix truncation order larger. Therefore, if the step in parameter, while being sufficiently small, is still by 1-2 orders larger than MAR's error, then these false resonances become "invisible." The false resonances can still be seen on the plots in Figs. 3 and 4 near to the frequencies of ka = 2.405 and 1.841, respectively - these are the lowest zeros of the Bessel functions and their derivatives, respectively.

However if the IE is discretized using a rougher scheme like a BEM or Galerkin MoM with local basis functions, then the domains of huge errors are much wider and overlap one another at the frequencies slightly larger than the first spurious-eigenvalue frequency. This makes any computations with such an algorithm completely senseless.

The full remedy is the use of the Muller IE which is completely equivalent to the original boundary-value problem and thus free of spurious eigenvalues.